Ge-Si alloy microstructure fabrication by direct-laser writing with analysis by Raman microprobe spectroscopy

Cite as: Journal of Applied Physics **61**, 5118 (1987); https://doi.org/10.1063/1.338286
Submitted: 24 September 1986 • Accepted: 02 February 1987 • Published Online: 04 June 1998

Irving P. Herman and Frank Magnotta

Ge-Si alloy microstructure fabrication by direct-laser writing with analysis by Raman microprobe spectroscopy

Irving P. Herman[a] and Frank Magnotta
Department of Physics, University of California, Lawrence Livermore National Laboratory, Livermore, California 94550

(Received 24 September 1986; accepted for publication 2 February 1987)

Micron-dimension structures of germanium-silicon alloys of various compositions are formed by several direct-laser writing techniques, including pyrolytic deposition of silicon from silane on laser-melted germanium substrates and codeposition from silane/germane mixtures on different absorbing substrates. *In situ* composition analysis of these polycrystalline alloy microstructures is performed by Raman microprobe analysis. The measured Raman shifts and widths of the laser-deposited alloys are found to be in better agreement with published Raman data on germanium-silicon alloy films than with the Raman data on alloy bulk solids. In the codeposition of alloys, the decomposition of germane to form Ge is observed to be about six times faster than the decomposition of silane to form Si, independent of the silane/germane ratio, laser power, and substrate type.

I. INTRODUCTION

The tunability of the optical, electrical, and structural characteristics of germanium-silicon alloys derived by varying alloy stoichiometry has spurred interest in the properties of these compounds and their potential applications. Use of these compounds for strained-layer superlattice and heterostructure devices,[1] epitaxial transition layers between GaAs structures and Si wafers,[2] and tunable band-gap solar cells[3] is drawing widespread attention. In most of these studies, thin films and multilayers of amorphous and crystalline $Ge_{1-x}Si_x$ have been deposited by plasma-assisted decomposition,[3] sputtering,[4] molecular-beam epitaxy,[1] or thermal mixing of predeposited films.[2] There has been relatively less recent work on Ge-Si alloy film preparation by chemical vapor deposition (CVD).[5,6] This paper examines several new approaches to the fabrication of micron-dimension Ge-Si alloys structures using direct-laser writing. The two main techniques investigated here are laser pyrolytic deposition (CVD) of silicon from silane on simultaneously locally laser-melted germanium substrates (forming a "melt alloy" after Si/Ge mixing), and the laser pyrolytic codeposition (CVD) of the alloy directly from silane/germane mixtures on various absorbing substrates ("codeposition alloy"). *In situ* analysis of the alloys is performed by Raman microprobe methods.[7] A brief, preliminary description of this work can be found in Ref. 8.

The first-order Stokes Raman spectrum of polycrystalline Ge-Si alloys consists of three distinct peaks near 300, 400, and 500 cm^{-1}, corresponding to local modes of Ge-Ge, Ge-Si, and Si-Si atom pairs, respectively. The central frequency, width, and relative integrated intensity of each peak has been investigated as a function of x, the silicon atomic fraction.[4,9,10] Raman measurements in Refs. 9 and 10 were made on hot-pressed or zone-leveled polycrystalline solids, while those in Ref. 4 were made on sputtered amorphous films which were recrystallized. As the silicon fraction of the bulk solid Ge-Si alloy increases from $x = 0$, the peak frequency of the Ge-Ge peak decreases from that of pure Ge ($x = 0$) 301 cm^{-1} to about 285 cm^{-1} (for $x = 0.8$); also its width rapidly increases.[9,10] Similarly, the frequency of the Si-Si peak decreases from the 520 cm^{-1} shift of pure Si ($x = 1$) to about 450 cm^{-1} (for $x = 0.1$) and the width also quickly increases, as the silicon content decreases from $x = 1$.[9,10] The Ge-Si local mode peak frequency lies in between these two peaks and attains a maximum of 407 cm^{-1} near the $x = 0.5$ state of the perfectly ordered $Ge_{0.5}Si_{0.5}$ alloy, and slowly decreases both for increasing and decreasing values of x. The width of this central peak is constant and small for $x < 0.5$, and then increases to a larger, yet fairly constant value for $x > 0.5$.[9,10] For each of the three alloy peaks, the measured linewidths appear to be much larger for the thin-film samples of Ref. 4, than for the bulk samples of Refs. 9 and 10. Also, the change in the x-x local frequency with added impurity, e.g., for Ge-Ge with added Si, is significantly smaller for the thin-film samples than for the bulk alloys. (These published $Ge_{1-x}Si_x$ alloy Raman data are depicted below in Figs. 3 and 4.)

To first order, the relative integrated Raman intensity of the three peaks is stoichiometrically based on the number of local atom pairs; i.e., the intensities of the peaks of the pairs vary as Ge-Ge:Ge-Si:Si-Si = $(1-x)^2$: $2x(1-x)$: x^2, assuming equal oscillator strengths.[4,9] More quantitative analysis is possible from the published spectra.[4]

Other factors are known to influence the $Ge_{1-x}Si_x$ alloy Raman spectrum. Stress introduces a shift in each of the three peaks, as noted in studies of hydrostatic stress on alloy solids and films[4,11] and of uniaxial stress in strained-layer structures.[12] Furthermore, sample stoichiometric inhomogeneity can broaden each peak. Alloy crystallinity also markedly affects the Raman profile. Specifically, amorphous alloys exhibit Raman peaks which are much broader, more poorly resolved, and less shifted in frequency than do polycrystalline germanium-silicon alloys of the same composition.[4] Finally, since the effective probe depth in Raman anal-

[a] Current address: Department of Applied Physics, Columbia University, New York, New York, 10027.

 0021-8979/87/115118-11$02.40

ysis is about half the absorption depth of the material, knowledge of alloy optical absorption is needed to determine the probe depth. At 5145 Å the absorption depth continuously varies with stoichiometry from $\sim 0.8\ \mu m$ for Si-rich alloys ($x \lesssim 1$) to $\lesssim 0.1\ \mu m$ for Ge-rich alloys ($x \gtrsim 0$) near 300 K (Ref. 13); at higher temperatures the absorption length and the corresponding probing depth of such indirect band-gap materials decrease rapidly.[14]

II. EXPERIMENTAL METHODS

In the experiments performed here, 5145-Å radiation from an argon-ion laser was focused by a microscope objective onto the substrate to about a 2-μm radius in an experimental arrangement similar to that reported in Ref. 7. The focused laser served to locally heat the substrate and induce surface-mediated pyrolysis from gas-phase reactants. Typically, $\sim$4-μm-wide and 1–3-μm-high microstructures were obtained using a scanning speed of 0.05 mm/s and laser powers ranging from 50 mW for thermally insulating substrates to 800 mW for thermally conducting substrates. The same laser was used for Raman scattering, both during deposition (real-time) and after deposition with the reactant removed (*in situ*). For microstructure analysis after deposition, the laser power could be varied to alter the microstructure temperature profile. Depending on the goal of the specific deposition experiment, either neat silane, neat germane, or a silane/germane mixture was introduced into the reaction cell, which included the substrate and an overlaying window to permit laser irradiation of the substrate. The fraction of silane content in the reactants x_M was set to be either 0, 25, 50, 75, 90, or 100%. The reactant pressure was fixed at 200 Torr in each experiment.

The substrates used in the various studies were *c*-Si, polycrystalline Ge, *a*-Si (on SiO_2/Si), vitreous carbon, graphite, molybdenum, and tantalum. Each of these substrates has an absorption depth much smaller than the focus diameter, thereby permitting efficient laser heating of the surface. At times, the microstructures formed by direct-laser writing were annealed *in situ* by laser heating in vacuum.

In situ Raman analysis was performed to determine the stoichiometry of the alloy microstructures. To avoid significant substrate heating during such analysis, only very low laser powers were used during probing < 20 mW for Ge and Si substrates. For these Raman microprobe measurements Stokes radiation, orthogonally polarized to the probe laser, was collected by the microscope objective and was transmitted through a set of four laser-line-absorbing filters to a single 1-m monochromator; it was then detected by an intensified, diode array scanning spectrometer.[7] Wing absorption in the laser line filters decreased the light collection efficiency at a 300 cm^{-1} Raman shift (near the Ge-Ge mode) by a factor of about 3–4 relative to that at 500 cm^{-1} (Si-Si mode). The necessary recalibration of the signal strength was employed in data analysis, though it is not incorporated in the Raman spectra displayed in the figures below. Similarly, peak frequencies and widths were corrected to zero laser power, as necessary. In some experiments electron-beam-induced x-ray energy-dispersive analysis was also used to determine alloy composition.

III. RESULTS AND DISCUSSION

A. Alloy formation

Germanium-silicon alloy microstructures were fabricated by following several different procedures. For silicon deposition on germanium substrates using silane as the reactant, experimental regimes could be found in which the alloy was formed, as indicated by the characteristic three-peak Raman spectrum, or in which only pure silicon was deposited, as suggested by the typical one-peak silicon spectrum. At faster scan speeds and lower laser powers only silicon was observed. Since in Si the Raman probe is sensitive to a depth of only about 0.4 μm (5145 Å, 300 K), it is still possible that some alloy is formed below the top silicon layer in the regimes in which only Si was observed. Figure 1(a) shows an SEM of one line microstructure of the melt alloy. The morphology of a purely silicon line obtained under slightly different experimental conditions was very similar. The fringes running down the center are parallel to the direction of travel and normal to the linear polarization of the laser.[15,16] There is also evidence of material buildup at either side of the line.

The Raman peak positions, widths, and strengths of the melt alloy imply that the melt alloy is polycrystalline.[4] Based on the laser-induced temperature rises deduced from the shift and broadening in the Raman spectra of laser-heated silicon microstructures,[7] it is reasonable to presume that the germanium substrate is melting ($T = 1210$ K) during deposition in this study. Under similar writing conditions with no silane present, visual changes observed with the laser microscope also suggest that the focused laser melts the Ge substrate. Overwriting the alloy with silane usually produced an overlayer of silicon.

Several attempts were made to produce Ge-Si alloys by writing pure Ge from germane on *c*-Si or *a*-Si. In each instance a germanium deposit was observed, but with no sign of the alloy. Since *c*-Si and *a*-Si melt at much higher temperatures ($T = 1690$ K and about 1450 K, respectively) than Ge and since germane decomposes at a lower temperature than silane, the writing conditions necessary to melt the substrate results in a thick germanium deposit. The shallow effective Raman probe depth of $\sim 0.05\ \mu m$ for pure germanium would easily mask any alloy layer if it were formed.

Ge-Si alloys were also codeposited from $x_M = 0$–1 silane/germane mixtures on Ge, *c*-Si, *a*-Si, vitreous carbon, graphite, Mo, and Ta. These substrates provided a range of different lattice matching and thermal conditions, yet each absorbed a large enough fraction of the incident radiation ($> 40\%$) within 1 μm of the surface to induce efficient surface heating. Figure 1(b) shows an SEM of the line microstructure formed from an $x_M = 0.75$ mixture on a Ge substrate. This double-ridged morphology, often seen in pyrolytic laser deposition of silicon and other materials,[16] is also observed here in alloys made from $x_M = 0.9$ mixtures and pure Ge deposits. (It has been shown that with judicious choice of experimental conditions silicon lines with flatter tops can be fabricated,[16] as is also expected here.) There is still evidence of fringes running parallel to the scanning direction. Codeposited lines overwritten four times were significantly wider than those with one write cycle, yet exhibit-

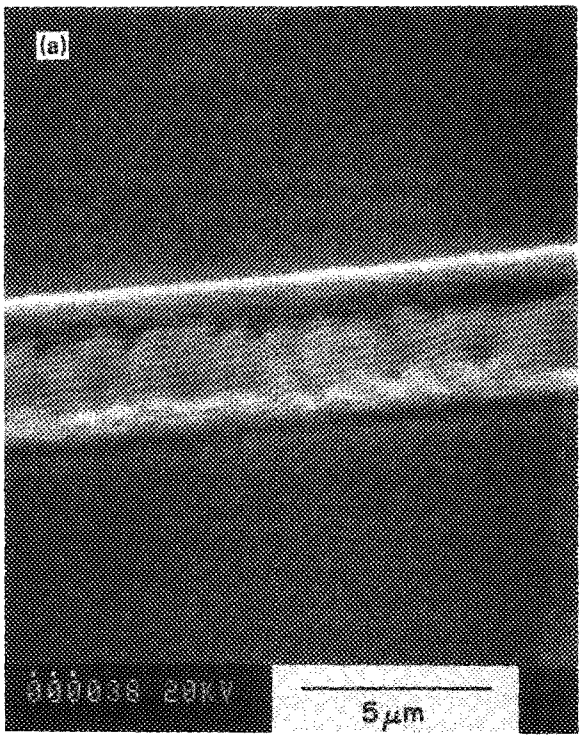

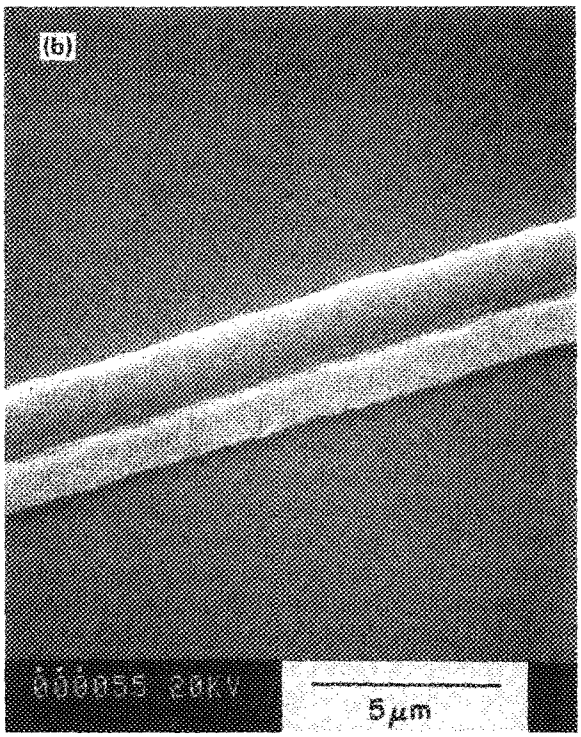

FIG. 1. SEM of (a) Ge-Si melt alloy formed using 200 Torr SiH_4 (view is 45° from vertical) and (b) Ge-Si codeposition alloy deposited from 150 Torr SiH_4/50 Torr GeH_4, $x_M = 0.75$ (view is at 30°). In both cases the Ge substrate is scanned at ~0.05 mm/s, relative to the 800 mW of 5145 Å argon-ion laser radiation, which is focused to a ~2-μm beam radius.

ed similar double-ridged morphology.

Visual inspection during writing showed that a deposit formed for each mixture/substrate combination. However, not all cases exhibited a Raman spectrum with measurable structure. For *c*-Si, polycrystalline Ge, Mo, and Ta substrates each mixture produced a microstructure with its characteristic three-peak spectrum. Figure 2 portrays the low-power (20 mW) spectrum of a codeposition alloy ($x_M = 0.75$) on Ge at one spot along a line. The Raman spectra for melt alloys look similar. Since in many experimental regimes the Raman spectra were virtually identical for codeposition on either Si or Ge substrates, there does not appear to be any mixing of the deposit with the substrate (i.e., melt alloying) in these cases, at least to the Raman probe depth. However, in some regimes there was evidence for slight melt alloying during codeposition of the alloy on Ge. In these cases an alloy line was codeposited on the Ge substrate and analyzed, and then was overwritten and analyzed again; the overwritten line had a slightly lower Ge content than the first line.

For *a*-Si surfaces, Raman signals were seen for silicon deposition from neat silane and sometimes also for deposition from mixtures containing germane. For vitreous carbon and graphite, spectral structure in the Raman signal was seen only for silicon deposition from neat silane. To further examine the nature of these deposits from silane/germane mixtures which have no measurable Raman signal within the sensitivity of the apparatus, x-ray dispersive analysis was performed for the deposits formed by laser CVD with $x_M = 0.25$, 0.50, and 0.75 reagent mixtures on vitreous carbon. This analysis confirmed that the deposits were indeed Ge-Si alloys. The distinction between the two cases appears to be that for the first set of substrates (*c*-Si, Ge, Mo, and Ta) all of the alloy deposits are polycrystalline, while for the second set of substrates (vitreous carbon and graphite) only the silicon deposit is polycrystalline and the alloy and pure germanium deposits are amorphous. Note that the second

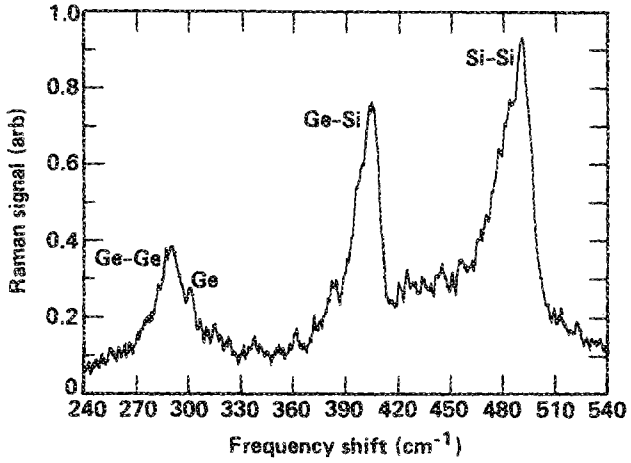

FIG. 2. Low laser power Raman spectrum of a codeposition alloy on a Ge substrate. The deposition mixture was $x_M = 0.75$, and x was determined to be 0.3. The peaks near 290, 400, and 480 cm^{-1} correspond to the Ge-Ge, Ge-Si, and Si-Si local modes respectively. The sharp peak near 300 cm^{-1} corresponds to the Ge substrate.

set of substrates are either amorphous or have a very different lattice structure vis-à-vis Ge-Si alloys. Attempts to recrystallize the amorphous alloys using *in situ* laser heating were not successful.

The writing rate of codeposition alloys was found to increase monotonically with increase in germane fraction in the mixture (i.e., decrease in silane and x_M). This was deduced from deposit cross-section measurements performed by profilometry and scanning electron microscopy.

Alloy formation was also demonstrated by first writing a Ge (Si) line by laser pyrolytic deposition, overwriting it with a Si (Ge) line, and then heating the structure with the laser with no reactive gas present.

B. Stoichiometry analysis

Raman spectra of the alloy microstructure probed at low laser power (<20 mW), such as the one shown in Fig. 2, should uniquely determine the composition of the alloy using at most two of the six data points available from the frequency and width of the three peaks. Furthermore, x should be obtainable independently from the ratio of the integrated Raman signal of any two of the three peaks. (The assumption that the local mode peak integrated intensity depends only on the fraction of local atoms pairs, was found to be only approximately true, based on the published Raman spectra.) Consistent values of x within ± 0.1 were typically obtained here by analyzing the central frequency of any of the three Raman peaks or the ratio of the integrated signal intensity of the two largest peaks.

The Raman spectra obtained here have the noted three-peak structure (Fig. 2) with the characteristic germanium-silicon alloy peak asymmetry, exhibiting a sharp rise on the high-frequency side and a slow tail on the low-frequency side, especially for the Ge-Si and Si-Si peaks. In many of these spectra there appear to be shoulders (indicating additional resonances) on the low-frequency side of the peaks, particularly for the Ge-Si and Si-Si modes. Also, there is a large background Stokes signal between the Ge-Si and Si-Si peaks, beyond that expected from the Si-Si profile asymmetry and peak overlap. These different features are apparent in Fig. 2.

Using this analysis procedure, the composition of several of the microstructures obtained during melt alloy writing was determined. The polycrystalline materials obtained in laser deposition of Si from SiH_4 on Ge range in composition from pure Si, through Si-rich alloys ($x \sim 0.8$), through to Ge-rich alloys ($x \sim 0.2$).

The silicon content in codeposition alloy microstructures fabricated using 90% SiH_4/10% GeH_4 mixtures ($x_M = 0.9$) over several runs was $x = 0.6 \pm 0.1$. Consequently, the ratio of the dissociation probability of GeH_4 to that of SiH_4 during laser CVD,

$$y = [(1-x)/x]/[(1-x_M)/x_M], \qquad (1)$$

is $y = 6 \pm 2$. For the 75%/25% mixture, $x = 0.3 \pm 0.1$, and $y = 7 \pm 3$ (Fig. 2). These values of x are found to be independent of the type of substrate, and are relatively insensitive to the exact writing conditions. Within experimental error, the same value of y is obtained for both values of x_M. Lines written with more germane-rich reactant mixtures ($x_M \leqslant 0.5$) appeared to be very nearly pure germanium according to Raman analysis.

Energy-dispersive x-ray analysis performed on the codeposition alloy microstructures written on vitreous carbon also suggests that y is independent of x_M. For deposits formed with $x_M = 0.25$, 0.50, and 0.75 mixtures, silicon fractions were $x = 0.086$, 0.20, 0.45 respectively, leading to $y = 3.8 \pm 0.2$, again independent of which mixture was used. In addition to this "x_M-dependent" precision deviation in determining y, a larger deviation of roughly ± 1.5, due to calibration uncertainties in the x-ray analysis (arising from the thin nature of the film and the nonflat topography of the alloy microstructures) limits accurate determination of y. Still, the value of y obtained here is consistent with those obtained above for polycrystalline Ge-Si alloys using Raman analysis. Measurements of deposition rate versus x_M for a series of runs on vitreous carbon with identical substrate scanning speed, laser focus, and laser power, also yielded values of y which are consistent with those obtained above.

In the only previous quantitative study of large-area codeposition of Ge-Si alloys by CVD of germane/silane mixtures,[5] the relative germane/silane dissociation probability y was $\simeq 1$ independent of flow rate and temperature, because deposition of both species was mass-transfer controlled. In the present study y is found to be independent of the relative silane/germane mixture ratio for each substrate and laser power tested, and more specifically, that value of y was found to be $\gg 1$. Since y is independent of x_M, silane and germane decomposition are probably independent of each other. This means that the radicals and atoms produced in the decomposition of one reactant (such as GeH_2, GeH_3, and H from GeH_4) do not significantly react homogeneously or heterogeneously with the other reactant (SiH_4). If the rate of these cross reactions of reaction products of one reactant with the other reactant (SiH_4) were competitive with the decomposition rate of the first reactant (GeH_4), y would be strongly pushed to a value near 1. Furthermore, since y is very different from 1, the deposition of codeposition alloy microstructures must be surface-reaction controlled, and not mass-transfer limited, in the present experiments.

The large values of y measured here are not surprising since at a given temperature, germane is expected to decompose faster than silane because of its weaker bonds. Extrapolation of the data for the surface-reaction limited CVD of *c*-Ge from germane[17] and of polycrystalline Si from silane[18] to about 800 K, suggests that Ge is deposited about 100 times faster than is Si for equivalent conditions at this temperature, even though the activation energy of both reactions is about 1.4 eV.[17,18]

The cited accuracy for the Raman determination of the alloy composition of ± 0.1 is not limited by the accuracy of peak frequency measurement, but by several other factors. Perhaps the most important is accurate knowledge of the Raman frequencies for the exact structure of the thin film microstructures written here. When comparing either the melt alloy or codeposition alloy Raman peak shifts with any of the three sets of published spectra,[4,9,10] small inconsistencies arise—most probably from the differing nature of alloy

preparation; this limits current consistency in determining x to about 0.1.

The Raman frequencies for Ge-Si bulk alloys in the studies of Renucci *et al.*[9] and Brya[10] are in rough agreement with each other; however, they significantly differ from the results of Ishidate *et al.*[4] for recrystallized sputtered amorphous films. These differences in the published data are illustrated in the compilation of curve fits to their respective data in Fig. 3. Analogous curve fits for the published Raman linewidth data are plotted in Fig. 4. The data in these two figures agree at the end points ($x = 0$ and $x = 1$), but deviate in between these points.

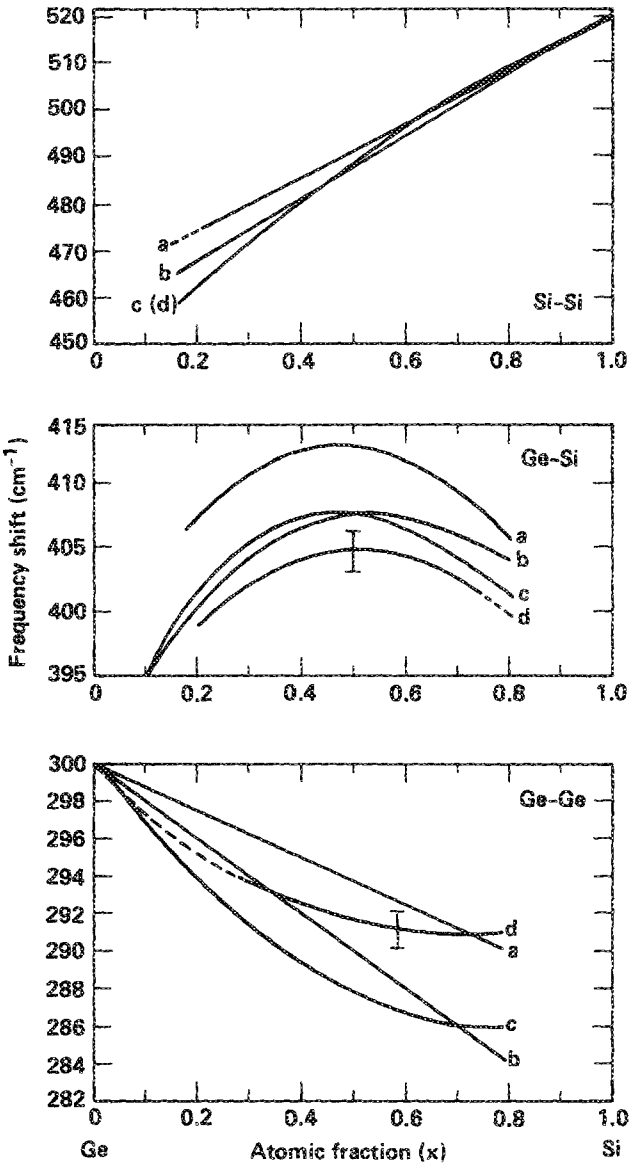

FIG. 3. Fits to the published data of Raman frequency shift vs alloy silicon atomic fraction x from (a) Ref. 4, (b) Ref. 10, and (c) Ref. 9, are plotted for the Si-Si, Ge-Si, and Ge-Ge local mode peaks. As described in the text, the current codeposition alloy data is also plotted for the Ge-Si and Ge-Ge peaks, as curve (d), presuming x assignments from the Renucci *et al.* (Ref. 9) Si-Si peak frequencies.

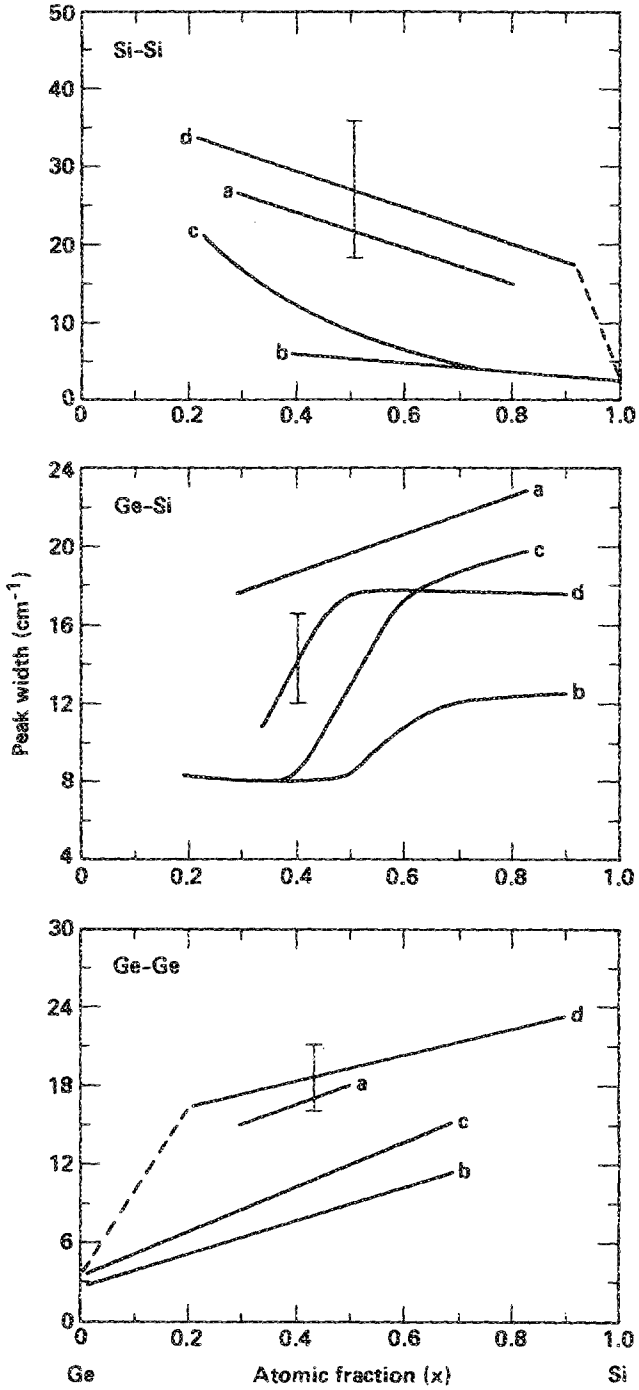

FIG. 4. Fits to the published data of Raman peak width vs alloy silicon atomic fraction x from (a) Ref. 4, (b) Ref. 10, and (c) Ref. 9 are plotted for the Si-Si, Ge-Si, and Ge-Ge peaks. The fits to the Raman spectra of the laser-written alloys are also plotted, as curve (d), using the Si-Si peak frequency (Ref. 9) assignment described in Fig. 3 and the text.

For comparison with these published results, the present data were analyzed as follows. Instead of determining x from the Raman shift of each of the three peaks and from the relative peak intensities as was done above, x values for the analyzed regions of laser-written alloys were uniquely determined from the Si-Si peak frequency using the data by Renucci *et al.*[9] This procedure was adopted because for each of the three sets of Raman data the Si-Si peak frequency deter-

mined from the Si-Si peak frequency using the data by Rennucci *et al.*[9] This procedure was adopted because for each of the three sets of Raman data the Si-Si peak frequency determines a unique value of x (unlike the Ge-Si peak which is bivalued) and has a far greater dynamic range (i.e., slope in Fig. 3) than either of the other two peaks, and also because the instrument response is highest in the Si-Si frequency range. The data fits for the Ge-Si and Ge-Ge local mode Raman shifts are plotted in Fig. 3, along with fits to the published spectra. Data from only the codeposition microstructures on Ge and c-Si, both after deposition and after laser annealing (see below), were used. The data have been corrected for the small temperature rise due to laser heating with 20-mW probe power, as described in Sec. III C. Use of the Si-Si data from Ref. 4 or 10, instead of those from Ref. 9, would have produced qualitatively similar results. Note that the present Ge-Si peak data seem more consistent with the shifts of the bulk alloy than with those of the thin film. The Raman shift of $Ge_{0.5}Si_{0.5}$ measured by Ishidate *et al.*[4] for the polycrystalline thin films is over 5 cm^{-1} higher than that measured either here or in the two bulk alloy studies.[9,10] However, the smaller slope of Ge-Ge peak frequency with x of the present work seems in best agreement with the thin-film data.

A similar analysis was performed for the widths of the Raman peaks, using both the codeposition and melt alloy data. The curve fit for the FWHM widths of each of the three peaks is plotted in Fig. 4 for the alloy microstructure data, with x determined from the Si-Si peak frequency as above. Fits to the data from Refs. 4, 9, and 10 are also plotted in this figure. The linewidths of the alloy Raman peaks for the film are typically 15 cm^{-1} or more and are consistently larger, at times two times larger, than those for the bulk alloy. However, the narrow 3–4 cm^{-1} linewidths for laser-written pure Si and pure Ge agree with the Raman spectra of the respective bulk solid samples. The large Raman widths measured here are much more consistent with the thin-film alloy data than with the bulk alloy data. Also, the x dependence of the present data and the thin-film data are also in rough agreement. Ishidate *et al.*[4] showed that for incompletely annealed thin films, further annealing may tend to narrow the Si-Si peak and not affect the Ge-Ge and Ge-Si peaks at all. The relatively large Si-Si peak widths measured here vis-à-vis the thin-film data and the large dispersion in the present data, suggest that the Si-Si peaks may be excessively wide because of incomplete annealing and that they may narrow further after annealing.

Several alloy microstructures were annealed in a vacuum furnace for 90 min at 800 °C, following the prescription of Ishidate *et al.*[4] for thin-film recrystallization and annealing. There was little, if any, change in peak widths; the Ge-Si and Ge-Ge peaks may have narrowed by about 1 cm^{-1}, while the width of the Si-Si feature was unchanged. The peaks widths were still within the variance bars, and were still larger than those in the published spectra.

Because of the similarities in Raman widths, the present spectra seem more similar to the thin-film alloy spectra than the bulk alloy Raman spectra. Still, there are some striking differences in the Raman shifts for these two cases. Raman measurements on CVD Ge-Si alloy films should help resolve this question of calibration. The Raman spectra of CVD films may differ from those of sputtered films because of different grain sizes and possible residual hydrogen in CVD-prepared thin films. For example, the three TO mode frequencies in hydrogenated a-GeSi are significantly higher than for the unhydrogenated alloy.[19]

Three other factors can influence stoichiometry analysis. Stress between the microstructure and the substrate can shift the Raman peaks, thereby complicating the determination of x. To test this, each of the three experimental peak frequencies was shifted by a few cm^{-1} and compared to the published Raman shifts; the precise relative shift for each peak was derived using the respective Gruneisen constants of the three peaks[4,11] or the respective peak stress-induced shift in strained-layer superlattices vis-à-vis unstrained material.[12] No significant improvement in assignment occurred. Also, stress-induced shifts in the Raman frequencies seem insignificant because the peak frequencies of codeposited alloys are essentially independent of substrate type. Similarly, codeposited alloy microstructures deposited on top of one another show no difference in peak frequencies. If stresses were important, significant differences would be observable. Furthermore, any such stress-induced spectral perturbations for Ge-Si alloys on Ge or Si should be much less than those for silicon microstructures on Ge substrates because of superior lattice matching in the former case. The stress shifts for Si lines on Ge are thought to be $\ll 2$ cm^{-1}.[7]

Another complication in determining the relative silicon/germanium content in the microstructures is the potential spatial variation in alloy composition, leading to averaging in the Raman microprobe analysis. One type of spatial variation is a slow gradient in composition across the line microstructure, with a characteristic distance of a micron. Because of the deposition, liquid mixing, and diffusion steps involved in melt alloy formation, it would be surprising if such gradients did not exist to some degree in that case. Another type of nonuniformity is a fluctuation in x on a much finer, local scale. One extreme example of this is the appearance of submicron aggregates of Si or Ge. (Such microaggregates are not thought to exist in bulk prepared Ge-Si alloys. Phonon spectra measurements have shown Ge-Si alloys to be configured in a randomly ordered diamond-type lattice in which alloy minority atoms occur only as next-nearest neighbors and not in clusters of similar atoms.[20]) To test these possibilities, averaged Raman spectra were calculated using the bulk alloy data of Rennuci *et al.*[9] by assuming a certain average value silicon content $\bar{x}$ with a Gaussian distribution dispersion about this average, for different dispersion widths Δx ($1/e$ halfwidth). The net Raman shifts and widths for these simulations are reproduced in Figs. 5 and 6. Although this averaging tends to broaden the peak widths, bringing them closer to the observed widths, overall peak frequency assignment was not significantly improved. Furthermore, Fig. 5 shows that for large composition gradients, $\Delta x = 0.3$, the Si-Si peak frequencies for small x never become smaller than roughly 480 cm^{-1}, in contrast to the experimentally observed values down to about 460 cm^{-1}. Finally, no evidence of pure Si or Ge microclusters was ever

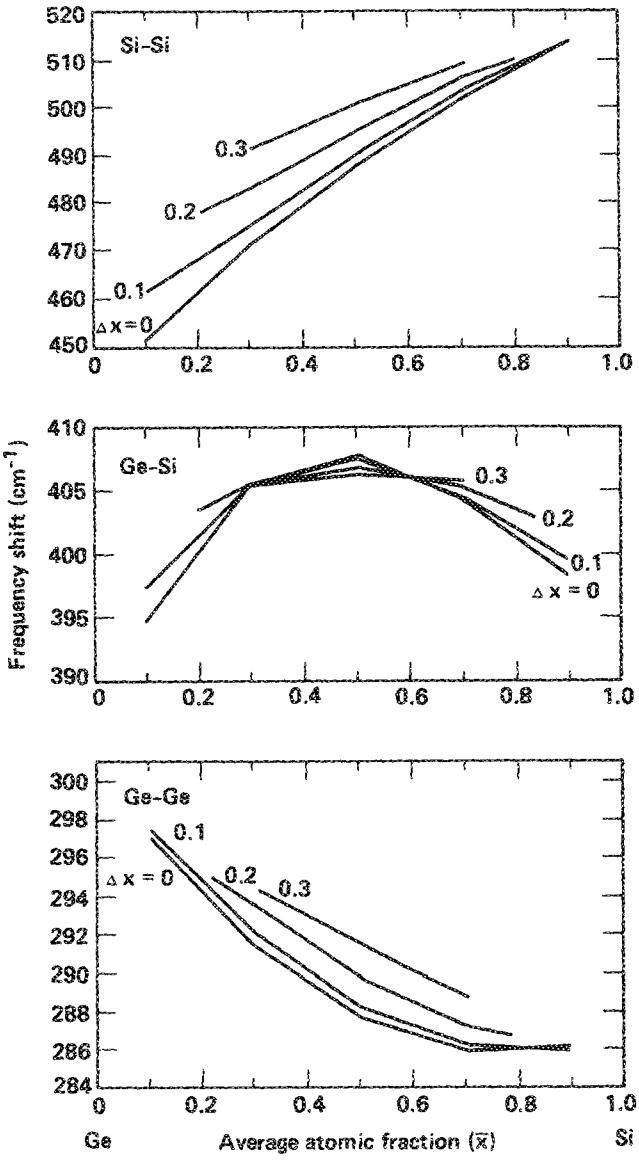

FIG. 5. Calculated peak frequencies vs average alloy composition $\bar{x}$, for simulations of Raman spectra of alloys with nonuniform composition, with $\bar{x} = 0.1, 0.3, 0.5, 0.7, 0.9$. The data of Ref. 9 are used, assuming an alloy composition distribution which is a Gaussian of $1/e$ halfwidth Δx about the average.

noticed in the Raman spectra of these Ge-Si alloys.

The third factor in composition analysis is crystallinity. The asymmetry in Ge-Si alloy Raman peaks has been attributed to the lack of translational symmetry in the random alloy and the concomitant relaxation of the $\Delta k = 0$ selection rule.[10] Furthermore, in polycrystalline materials with grain sizes less than 100 Å the translational symmetry aproximation is even more strongly violated, leading to a further increase in peak linewidth and asymmetry, and decrease in peak frequency, as demonstrated for polycrystalline Ge, Si, and GaAs.[21] (No measurement of grain sizes is reported here.) The observation of additional peak broadening (Fig. 4) and the appearance of additional resonances, noted above as shoulders on the low-frequency sides of the Si-Si and Ge-Si Stokes peaks, may be due to regions of different crystallinity—such as localized pockets with different grain sizes.

The large background between the Ge-Si and Si-Si peaks near 450 cm^{-1} suggests that there is a broad underlying peak in this region, possibly due to a-Si, or the Si-Si peak in a-GeSi or microcrystalline GeSi. This broad background remained even after oven annealing. However, based on the rates of random recrystallization of a-Si by Olson and co-workers[22] and the conclusion reached in Ref. 4 that a-GeSi completely recrystallized after oven annealing, it seems that any amorphous phase should have recrystallized as a result of this annealing cycle. (Since the broad background between the Ge-Si and Si-Si peaks remained in Ref. 4 even after annealing, this presumption that no amorphous or microcrystalline Ge-Si remained after oven annealing may not be valid.) It is also possible that the relatively weak, unassigned peaks in this 450 cm^{-1} region noticed by Byra,[10] which were fairly

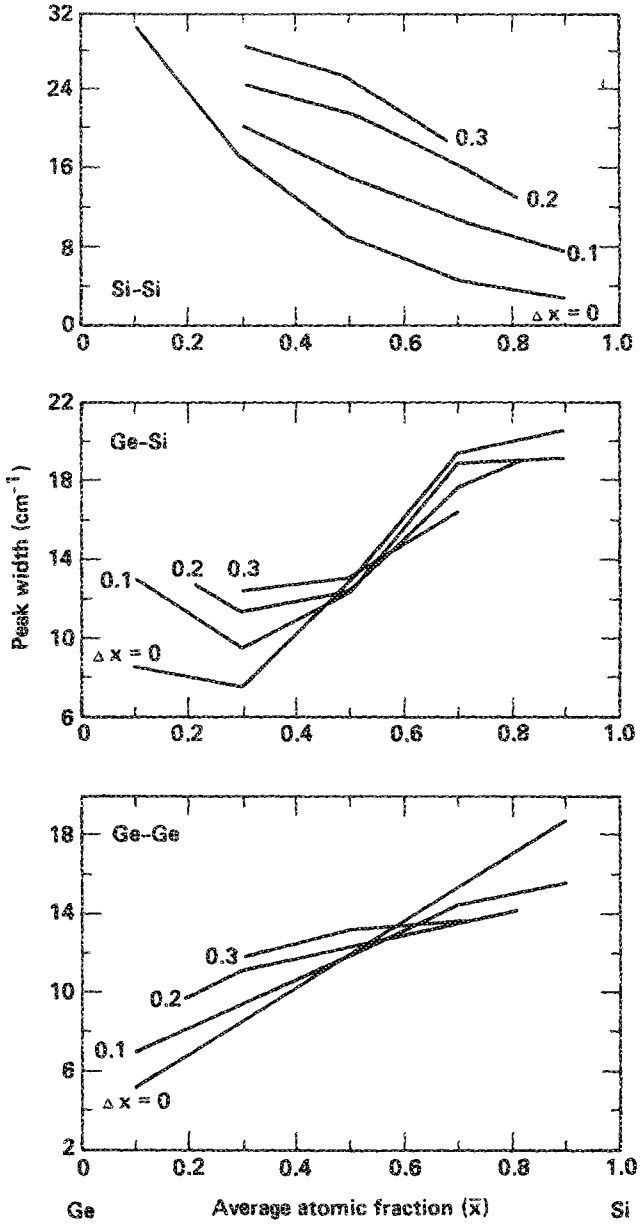

FIG. 6. Calculated Raman peak widths vs average alloy composition $\bar{x}$, for simulations of Raman spectra of alloys with nonuniform composition, as detailed in the Fig. 5 caption.

independent of x, may have a similar origin to the background observed here. Since this background appears only when the Ge-Si and Si-Si peaks are close in frequency (small x), it may, in fact, be due to a mixing of the Ge-Si and Si-Si resonances.

C. Irradiation and analysis of alloys at higher laser powers

1. Laser annealing

After deposition of a melt or codeposition alloy line, the reactant was removed and various spots on the microstructures were subjected to laser heating by a static, nonscanning focused laser in vacuum. In part, this was done to survey potential laser annealing effects. A typical laser heating sequence began with Raman microprobe analysis at the chosen spot at low power (<20 mW on Si or Ge) for an initial reference. Then the spot was heated using a specific high power (the annealing laser power) for several minutes, during which time the Raman spectrum was recorded. Afterwards, the same spot was irradiated with successively lower laser powers, with the Raman signal again recorded each time, until the initial low power, room temperature probe run is repeated. Such a sequence permitted observation of changes due to annealing, and also allowed measurement of the laser-power dependence of the Raman spectrum for a spot that had already been annealed. The spectra from one such sequence is shown in Fig. 7 for a 75%/25% codeposition alloy.

There were three regimes of effects, depending on the choice of annealing laser power. At very high powers (>400 mW), there were gross local physical changes in the microstructure due to melting and vaporization, effects which are not very interesting. The intermediate regime of annealing laser power was characterized by minor visual modification of the spot which was sometimes accompanied by a change in stoichiometry, as determined by Raman analysis. In the lowest regimes of annealing laser power (<250 mW) there were no noticeable physical changes. Attempts to laser anneal samples were conducted at the uppermost power in this lowest laser power range.

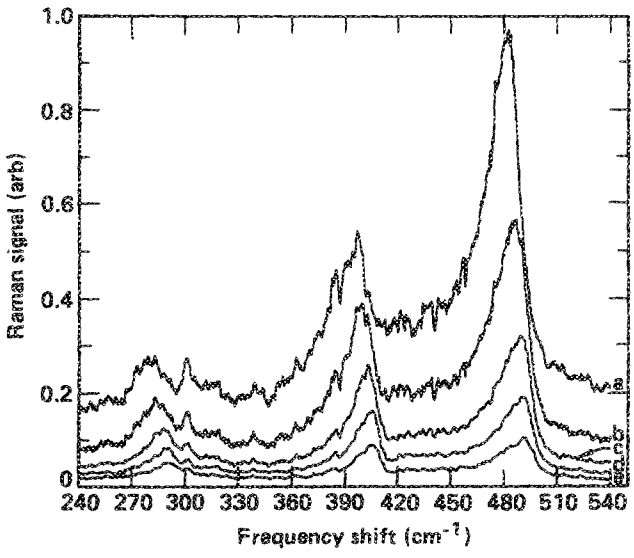

FIG. 7. Raman spectrum of a codeposition alloy ($x_M = 0.75$, $x = 0.3$) as a function of probing laser power, for (a) 250 mW, (b) 150 mW, (c) 75 mW, (d) 40 mW, and (e) 20 mW. The lowest laser power spectrum is the same as the one shown in Fig. 2. Note the peak near 300 cm^{-1} due to the Ge substrate does not change much in frequency with laser power.

The Raman spectrum recorded after such a low-power regime anneal was either identical to or only slightly modified from the pre-anneal and oven-treated spectra, based on a comparison of peak frequencies, widths, and absolute peak intensities. This was true for both melt and codeposition alloys. In some cases the Si-Si peak did narrow a little, but still the width of the Ge-Ge, Ge-Si, and Si-Si peaks remained 15–25 cm^{-1}, comparable to those of the annealed alloy films in Ref. 4 and much wider than those measured for the bulk samples in Refs. 9 and 10. Since the laser-induced temperature rises (to just below melting) and annealing times (1–4 min at a given $\sim$4-μm-diam spot) should have been sufficient to recrystallize any local concentrations of amorphous Ge-Si alloy, the observation that the Raman strength was the same before and after annealing should imply that the initial material was entirely polycrystalline and not a mixture of polycrystalline and amorphous regions. However, the abnormally wide and asymmetric peaks also suggest that the deposited material may be microcrystalline, with very small grain sizes that do not grow substantially upon annealing. Also, the possibility of some residual amorphous region cannot be absolutely ruled out. Regarding another possible effect of annealing, any microstructure-substrate stress relaxation resulting from annealing would have been indicated by a roughly equal (within a factor of about 2) translation of each of the three Raman peaks. No such behavior was ever observed.

Irradiating codeposited alloys with the intermediate range of laser power for 1–4 min sometimes produced large changes in alloy composition, as probed by the Raman technique, with minor observable structural modifications. At times laser irradiation tended to increase either the germanium or silicon content in the Raman probed surface layers of the microstructure. This was observed for such microstructures on c-Si or Ge substrates. No obvious correlation of enhanced surface Si or Ge with laser power, substrate type, alloy composition, or fabrication method (melt versus codeposition) was noted. No lateral diffusion of the alloy into adjacent regions or any other modification of the adjacent regions was noted in any of these annealing cases.

From the phase diagram for Ge-Si alloys,[23] it is known that at equilibrium the molten portion is relatively Ge rich, while the solid phase is Si rich. Depending on the specific microstructure and laser conditions, the molten-Ge-rich phase possibly may migrate to the microstructure surface and remain there after cooling, leaving a Ge-rich overcoating after cooling in some cases. There is no apparent reason to expect the molten region to always migrate to the surface. However, preferred segregation of Ge from large-area Ge-Si alloy thin films to the surface has been observed by Farrell and co-workers[24] after annealing and ion bombardment.

2. Thermal effects in the Raman spectrum

Figure 7 depicts a series of Raman spectra for a range of incident laser powers impinging at one spot along a codeposition alloy line. Similar spectra were obtained for laser heated melt alloys. Consistent with the procedure outlined above, these series of runs were conducted with descending laser powers; there was no apparent annealing of the spot during irradiation. As the laser power used in the probe increases the frequencies of each of the three local peaks decreases and the Ge-Ge peak becomes relatively weaker than the Si-Si peak. The width of each peak remains fairly constant, independent of laser power.

The decrease in peak frequency with increasing laser power corresponds to a decrease in each of the three Raman shifts with temperature. This type of temperature dependence is anticipated from the Raman Stokes spectra of oven-heated c-Si (Refs. 25 and 26) and c-Ge,[26] although it has never been observed previously for Ge-Si alloys. Figure 8 plots the frequency of each of the three peaks as a function of incident laser power for the data in Fig. 7. The nearly linear decrease in Raman shift with probe power portrayed in Figs. 7 and 8 was exhibited by all codeposition and melt alloys so examined. Because of the lack of previous Raman alloy data at elevated temperatures and because the profile of the temperature increase on the alloy surface induced by laser heating is not spatially uniform, no direct relation between Raman shift and temperature can be made here. Still, some semiquantitative conclusions may be drawn from this data. For one, the plots in Fig. 8 along with other similar data from other runs suggest that the peak frequencies measured with 20 mW are about 0.5 cm^{-1} lower than the zero power values. (As seen below, this corresponds to an average temperature rise of about 20 K during low-power probing.)

Over the range of incident laser power used in Fig. 7, the Si-Si peak frequency decreases by about 40 cm^{-1}/W or about 10 cm^{-1} for this 0–250 mW variation. If the change in the Raman shift of the Si-Si peak with temperature is assumed to be the same as that of c-Si,[25,26] which has a roughly -0.023 cm^{-1} shift per degree K in the temperature range of interest, then this variation of incident laser power corresponds to a local temperature range of roughly 300–800 K. If instead, the relative c-Si/Si-Si changes in Raman shift with temperature are scaled by their respective Raman shifts at 300 K, these temperature estimates are then barely modified. These same temperature estimates are also obtained if the temperature dependence of the Ge-Ge alloy peak is assumed to be the same as for c-Ge.[26] Since the temperature profile of the microstructure induced by laser heating is spatially nonuniform, the actual peak microstructure temperatures are really higher than these values,[7] with the maximum value perhaps 900–1000 K. Apparently, observable damage to the microstructure occurs at somewhat higher laser powers and correspondingly higher temperatures than these, near the melting temperature of the Ge substrate and the Ge-Si alloy lines.

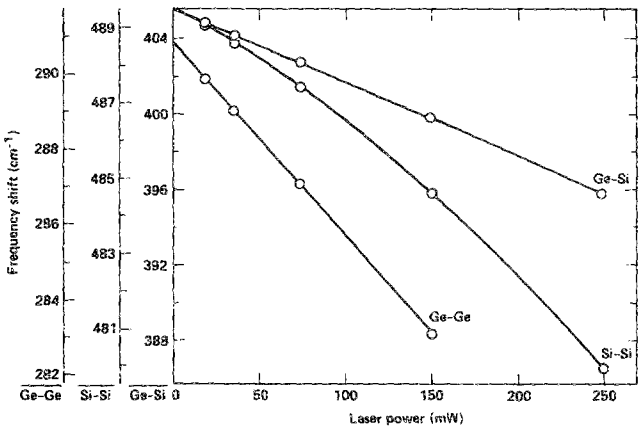

FIG. 8. Peak frequencies of the Si-Si, Ge-Si, and Ge-Ge peaks are plotted as a function of incident laser power for the data portrayed in Fig. 7. Note that there are different ordinate scales for each of the three peaks, with individual offset frequencies and expansions of the frequency scale.

This Si-Si peak/c-Si and Ge-Ge peak/c-Ge analogy can be extended to an examination of Raman widths with the following model. If the temperature-dependent portion of the linewidth, of, say, the Si-Si peak of the alloy, is identified with the width of the crystalline form of the element analog $\gamma_1(T)$, in this case c-Si, then the residual contribution to the linewidth (beyond the c-Si portion at 300 K, due to crystallinity effects, etc.) γ_2 may be assumed to be temperature independent in this model. Assuming that each broadening mechanism can be represented by a Lorentzian profile, then for the overall linewidth Γ: $\Gamma(T) = \gamma_1(T) + \gamma_2$. This should also be approximately valid for asymmetric Lorentzian line shapes. From the properties of c-Si, the temperature-dependent contribution γ_1 for the Si-Si mode of the alloy would be 2.5 cm^{-1} at 300 K and about 8 cm^{-1} at 800 K.[25,26] Since from Fig. 4 Γ (300 K) $\sim$ 25 cm^{-1} for this mode at $x = 0.5$, then $\gamma_2 \sim 22.5$ cm^{-1} and one would predict Γ(800 K) $\sim$ 30.5 cm^{-1}. For Ge the analogous values are γ_1(300 K) = 2.5 cm^{-1}, γ_1(800 K) = 7 cm^{-1},[26] and Γ(300 K) = 18 cm^{-1} (for $x \sim 0.5$ from Fig. 4), leading to $\gamma_2 \sim 15.5$ cm^{-1} and the predicted Γ(800 K) $\sim$ 22.5 cm^{-1}. However, this model-predicted increase in linewidth of about 5 cm^{-1} for each peak as the probe power is increased in Fig. 7, is not observed for either the Si-Si or Ge-Ge mode, since essentially no increase in linewidth is observed. Even if the polycrystalline alloy had residual amorphous regions, this model should be reasonable. For such a mixed phase material, the temperature dependence of the material would depend on two factors: on the linewidths of the crystalline and amorphous phases, and on the changing difference in phonon frequencies with temperature for these two phases. This latter effect is not important for Si.[27]

As the laser power and corresponding temperature rise increase, the integrated intensity of the Si-Si peak increases rapidly, while the intensity of the Ge-Ge peak increases much more slowly. The Ge-Si peak displays an intermediate behavior, more closely mimicking the Ge-Ge peak. The Stokes scattering probability, defined as the integrated intensity per incident photon, decreases only very slowly with increased laser power (temperature) for the Si-Si peak (by $\sim 30\%$ over the laser power range in Fig. 7 and other similar runs), while it decreases much faster for the Ge-Si (by a factor of ~ 2.5) and Ge-Ge peaks (by ~ 3.5). This is similar

to the behavior of laser-heated Si and Ge microstructures, for which the scattering probability was observed to decrease slowly with increasing laser power (temperature) for c-Si, and to decrease much more rapidly with power for Ge.[7] Again, this in accord with the dependence anticipated using the Si/Si-Si alloy mode, Ge/Ge-Ge alloy mode analogy. The ratio of Ge-Ge/Si-Si peak intensities in Fig. 7 (and in other similar runs) decreases by ~ 2.5 as the probe laser power is increased from low powers (300 K) to high laser powers (corresponding to ~ 800 K average temperature). The Stokes Raman scattering probability per incident photon in uniformly, oven-heated c-Si is known to decrease slowly with increasing T roughly as $\exp[-(T-293\ \mathrm{K})/T_0]$, where $T_0 \simeq 690$ K for 5145 Å.[28] Using this expression and the average local temperature of the laser-heated alloy microstructure of ~ 800 K for 250 mW (derived assuming the c-Si/Si-Si mode Raman shift analogy), a $\sim 50\%$ drop in Si-Si Raman Stokes probability would be expected, compared to the 30% drop observed here.

The Stokes Raman scattering rate for the X–Y local mode is R (Ref. 28):

$$R^{X-Y} = \left(\frac{\tilde{T}_S \tilde{T}_L P_L \nu_S^3}{(\alpha_L+\alpha_S)\eta_L\eta_S}\right)\left(\frac{\Delta\Omega[n(\omega_{X-Y})+1]}{32\pi^2 c^4 \omega_{X-Y}}\right) \times |\epsilon_L \epsilon_S \chi_{X-Y}|^2, \tag{2}$$

where the S and L subscripts refer to the Stokes and laser, respectively, $\tilde{T}$ is the transmission coefficient at the surface, P is the laser power, ν_S is the Stokes shifted optical frequency, α is the absorption coefficient, η is the index of refraction, $\Delta\Omega$ is the collection solid angle, ω_{X-Y} is the phonon frequency for local mode $X-Y$, $n(\omega_{X-Y})$ is the phonon-occupation factor for that local mode $[\exp(\hbar\omega_{X-Y}/kT)-1]^{-1}$, ϵ is the dielectric constant, and χ_{X-Y} is the Raman susceptibility for that mode. Although each of the materials parameters is a function of temperature, only α, n (ω), and χ have a particularly strong temperature dependence.

For a given alloy sample, the relative integrated intensity for the three peaks as a function of temperature depends only on the factor

$$[n(\omega_{X-Y})+1]\,|\chi_{X-Y}|^2, \tag{3}$$

because the other material-dependent terms, such as the absorption coefficient, are overall material properties and therefore are the same for each local mode. Since

$$\omega_{\text{Ge-Ge}} < \omega_{\text{Ge-Si}} < \omega_{\text{Si-Si}} \tag{4}$$

for all T under examination, it follows that

$$n(\omega_{\text{Ge-Ge}}) > n(\omega_{\text{Ge-Si}}) > n(\omega_{\text{Si-Si}}) \tag{5}$$

and

$$\frac{dn(\omega_{\text{Ge-Ge}})}{dT} > \frac{dn(\omega_{\text{Ge-Si}})}{dT} > \frac{dn(\omega_{\text{Si-Si}})}{dT}. \tag{6}$$

Using these relations and the experimental observations some qualitative statements can be made concerning the temperature dependence of the Raman susceptibilities in the frequency shift regime of the three Ge-Si peaks at 5145 Å for roughly the 300–800 K temperature range. (χ is assumed to be >0 here.) Since the Raman scattering rate for each mode decreases with temperature, using Eqs. (2) and (6):

$$\frac{dR^{X-Y}}{dT} < 0, \tag{7a}$$

leading to

$$\frac{d}{dT}\left(\frac{\chi_{X-Y}^2}{\alpha_L+\alpha_S}\right) < -\frac{1}{[n(\omega_{X-Y})+1]}\frac{dn(\omega_{X-Y})}{dT} \times\left(\frac{\chi_{X-Y}^2}{\alpha_L+\alpha_S}\right) \tag{7b}$$

and

$$\frac{d\chi_{X-Y}}{dT} < \frac{\chi_{X-Y}}{2}\left(-\frac{1}{[n(\omega_{X-Y})+1]}\frac{dn(\omega_{X-Y})}{dT} + \frac{1}{(\alpha_L+\alpha_S)}\frac{d(\alpha_L+\alpha_S)}{dT}\right), \tag{7c}$$

where the first term on the right-hand side of Eq. (7c) is negative and is straightforward to calculate (neglecting the slow temperature dependence of ω_{X-Y}), while the second term is positive and may be roughly estimated from the Ref. 14 data for Si.

Furthermore, since the ratio of the Raman scattering probabilities for the Ge-Si and Si-Si (and also for the Ge-Ge and Ge-Si) local modes is observed to decrease with temperature, for the mode pairs A-B /C-D = Ge-Ge/Ge-Si, Ge-Si/Si-Si, or Ge-Ge/Si-Si:

$$\frac{d}{dT}\left(\frac{R^{A-B}}{R^{C-D}}\right) < 0, \tag{8a}$$

or using relation (3):

$$\frac{d}{dT}\left(\frac{n(\omega_{A-B})+1}{n(\omega_{C-D})+1}\frac{\chi_{A-B}^2}{\chi_{C-D}^2}\right) < 0, \tag{8b}$$

and then using Eq. (6):

$$\frac{1}{\chi_{A-B}}\frac{d\chi_{A-B}}{dT} - \frac{1}{\chi_{C-D}}\frac{d\chi_{C-D}}{dT} < -\frac{1}{2}\frac{d}{dT}\ln\left(\frac{n(\omega_{A-B})+1}{n(\omega_{C-D})+1}\right) < 0, \tag{8c}$$

where the right-hand side is straightforward to calculate.

3. Real-time monitoring of alloy formation

The Raman spectra obtained in real-time during writing were also monitored. They were similar to those obtained post-deposition with the same laser power, and resembled the high-laser power Raman spectra in Fig. 7. Consistent with this observation, the Si-Si peaks were typically larger than the Si-Ge and Ge-Ge peaks even when Ge-rich alloys were written. Monitoring the real-time spectrum was particularly useful in determining whether melt alloys were being formed during the pyrolytic deposition of Si on Ge.

IV. CONCLUDING REMARKS

Several methods of thermally induced localized Ge-Si alloy fabrication have been investigated here. Pyrolytic silicon deposition on simultaneously-laser-melted Ge produced Ge-Si alloys with compositions ranging from highly Si-rich to highly Ge-rich stoichiometries. In the codeposition of al-

loys from silane/germane mixtures, the germane reactant decomposed approximately six times faster than the silane. This observation was independent of silane/germane ratio, laser power, and the details of the absorbing substrate. However, the crystallinity of the Ge-Si depended strongly on the substrate properties. Of those direct-laser writing techniques investigated here, the most reliable method of Ge-Si alloy formation is probably codeposition from silane/germane mixtures, especially on substrates which do not melt during laser chemical vapor deposition.

Raman microprobe analysis proved to be a valuable *in situ* diagnostic of the Ge-Si alloy properties. Some uncertainties in the determination of the alloy stoichiometry using this technique were noticed, which were attributed to the dependence of the Si-Si, Ge-Si, and Ge-Ge local mode Raman shifts and peak widths on the nature of the alloy morphology.

ACKNOWLEDGMENT

This work was performed under the auspices of the U. S. Department of Energy by the Lawrence Livermore National Laboratory under contract number W-7405-ENG-48.

[1]J. C. Bean, Science **230**, 127 (1985), and references cited therein.
[2]J. C. C. Fan, R. P. Gale, F. M. Davis, and G. H. Foley, Appl. Phys. Lett. **37**, 1024 (1980).
[3]K. D. Mackenzie, J. R. Eggert, D. J. Leopold, Y. M. Li, S. Lin, and W. Paul, Phys. Rev. B **31**, 2198 (1985); D. Della Sala, C. Giovanella, and F. Evangelisti, Phys. Status Solidi B **126**, 125 (1984).
[4]T. Ishidate, S. Katagiri, K. Inoue, M. Shibuya, K. Tsuji, and S. Minomura, J. Phys. Soc. Jpn. **53**, 2584 (1984).
[5]G. M. Oleszek and R. L. Anderson, J. Electrochem. Soc. **120**, 554 (1973).
[6]L. I. Halberg and J. H. Nevin, J. Electron. Mater. **11**, 779 (1982).
[7]F. Magnotta and I. P. Herman, Appl. Phys. Lett. **48**, 195 (1986); I. P. Herman, F. Magnotta, and D. E. Kotecki, J. Vac. Sci. Technol. A **4**, 659 (1986).
[8]F. Magnotta and I. P. Herman, Materials Research Society 1986 Fall Meeting—Final Program and Abstracts, Abstract D 6.3 (Materials Research Society, Pittsburgh, 1986), p. 133.
[9]M. A. Renucci, J. B. Renucci, and M. Cardona, in *Proceedings of the Conference on Light Scattering in Solids*, edited by M. Balkanski (Flammarion, Paris, 1971), p. 326.
[10]W. J. Brya, Solid State Commun. **12**, 253 (1973).
[11]J. B. Renucci, M. A. Renucci, and M. Cardona, Solid State Commun. **9**, 1651 (1971).
[12]F. Cerdeira, A. Pinczuk, J. C. Bean, B. Batlogg, and B. A. Wilson, Appl. Phys. Lett. **45**, 1138 (1984); J. Vac. Sci. Technol. B **3**, 600 (1985).
[13]R. Braunstein, A. R. Moore, and F. Herman, Phys. Rev. **109**, 695 (1958).
[14]G. E. Jellison, Jr. and F. A. Modine, Appl. Phys. Lett. **41**, 180 (1982).
[15]Zhou Guosheng, P. M. Fauchet, and A. E. Siegman, Phys. Rev. B **26**, 5366 (1982).
[16]D. Bauerle, in *Laser Processing and Diagnostics—Springer Series in Chemical Physics Vol. 39*, edited by D. Bauerle (Springer, Berlin, 1984), p. 166.
[17]H. Krautle, P. Roentgen, and H. Beneking, J. Cryst. Growth **65**, 439 (1983).
[18]A. M. Beers and J. Bloem, Appl. Phys. Lett. **41**, 153 (1982).
[19]P. K. Banerjee, R. Dutta, S. S. Mitra, and D. K. Paul, J. Non-Cryst. Solids **50**, 1 (1982).
[20]R. A. Logan, J. M. Rowell, and F. A. Trumbore, Phys. Rev. **136**, 1751 (1964).
[21]K. K. Tiong, P. M. Amitharaj, F. H. Pollak, and D. E. Aspnes, Appl. Phys. Lett. **44**, 122 (1984); J. Gonzalez-Hernandez, G. H. Azarbayejani, R. Tsu, and F. H. Pollack, Appl. Phys. Lett. **47**, 1350 (1985).
[22]J. A. Roth, S. A. Kokorowski, G. L. Olson, and L. D. Hess, in *Laser and Electron-Beam Interactions with Solids—Materials Research Society Proceedings, Vol. 4*, edited by B. R. Appleton and G. K. Celler (Elsevier, New York, 1982), p. 169.
[23]M. Hansen, *Constitution of Binary Alloys* (McGraw-Hill, New York, 1958), p. 774.
[24]H. H. Farrell, J. Q. Broughton, J. A. Schaefer, and J. C. Bean, J. Vac. Sci. Technol. A **4**, 123 (1986), and references cited therein.
[25]M. Balkanski, R. F. Wallis, and E. Haro, Phys. Rev. B **28**, 1928 (1983).
[26]J. Menendez and M. Cardona, Phys. Rev. B **29**, 2051 (1984) and references cited therein.
[27]R. Tsu and J. G. Hernandez, Appl. Phys. Lett. **41**, 1016 (1982).
[28]A. Compaan and H. J. Trodahl, Phys. Rev. B **29**, 793 (1984); A. Compaan, M. C. Lee, and G. J. Trott, Phys. Rev. B **32**, 6731 (1985).